AUTOPHAGY
2017, VOL. 13, NO. 1, 57–69
http://dx.doi.org/10.1080/15548627.2016.1241924

Taylor & Francis
Taylor & Francis Group

BASIC RESEARCH PAPER

The STX6-VTI1B-VAMP3 complex facilitates xenophagy by regulating the fusion between recycling endosomes and autophagosomes

Takashi Nozawa, Atsuko Minowa-Nozawa, Chihiro Aikawa, and Ichiro Nakagawa

Department of Microbiology, Graduate School of Medicine, Kyoto University, Kyoto, Japan

ABSTRACT

Macroautophagy/autophagy plays a critical role in immunity by directly degrading invading pathogens such as Group A *Streptococcus* (GAS), through a process that has been named xenophagy. We previously demonstrated that autophagic vacuoles directed against GAS, termed GAS-containing autophagosome-like vacuoles (GcAVs), use recycling endosomes (REs) as a membrane source. However, the precise molecular mechanism that facilitates the fusion between GcAVs and REs remains unclear. Here, we demonstrate that STX6 (syntaxin 6) is recruited to GcAVs and forms a complex with VTI1B and VAMP3 to regulate the GcAV-RE fusion that is required for xenophagy. STX6 targets the GcAV membrane through its tyrosine-based sorting motif and transmembrane domain, and localizes to TFRC (transferrin receptor)-positive punctate structures on GcAVs through its H2 SNARE domain. Knockdown and knockout experiments revealed that STX6 is required for the fusion between GcAVs and REs to promote clearance of intracellular GAS by autophagy. Moreover, VAMP3 and VTI1B interact with STX6 and localize on the TFRC-positive puncta on GcAVs, and are also involved in the RE-GcAV fusion. Furthermore, knockout of *RABGEF1* impairs the RE-GcAV fusion and STX6-VAMP3 interaction. These findings demonstrate that RABGEF1 mediates RE fusion with GcAVs through the STX6-VAMP3-VTI1B complex, and reveal the SNARE dynamics involved in autophagosome formation in response to bacterial infection.

ARTICLE HISTORY
Received 17 March 2016
Revised 12 September 2016
Accepted 22 September 2016

KEYWORDS
autophagy; Group A *Streptococcus*; RABGEF1/RABEX5; STX6 (syntaxin 6); xenophagy

Introduction

Autophagy is a lysosomal degradation pathway that degrades cytoplasmic components, including protein aggregates, damaged organelles, and invading bacteria. This pathway is essential for cellular homeostasis, survival, development, and host defense. During autophagy, a flat membrane structure, called the phagophore, is generated from or close to the endoplasmic reticulum and surrounds a portion of the cytoplasmic content, forming a closed double-membrane structure, the autophagosome. The process of autophagosome formation is regulated by autophagy-related (ATG) proteins, and one of the ATG proteins, MAP1LC3/LC3 (mammalian homolog of Atg8 in yeast), specifically localizes on phagophores and autophagosomes; the autophagosomes subsequently fuse with lysosomes and form the autolysosome, a lysosomal vacuole in which the autophagosome contents are degraded.[1,2]

Autophagy not only degrades a cell's own components, but also targets invading microbial pathogens. This antimicrobial autophagy, which is named xenophagy,[3,4] has been recognized as a crucial intracellular immune system against various pathogens, such as *Salmonella* Typhimurium and Group A *Streptococcus* (GAS).[4,5] GAS, one of the major human pathogens, enters epithelial cells through endocytosis and then escapes into the cytoplasm by secreting streptolysin O, a pore-forming toxin produced by GAS.[6] The exposed GAS in the cytoplasm is recognized by the ubiquitin-binding receptor proteins SQSTM1/p62 and CALCOCO2/NDP52 and entrapped by an LC3-positive autophagic membrane structure, the GAS-containing autophagosome-like vacuole (GcAV). RAB7 and RAB9A facilitate the homotypic fusion between GcAVs that generates large GcAVs,[7,8] and RAB9A mediates the fusion of GcAVs with lysosomes, which results in the degradation of the entrapped bacteria.[8] Recently, we showed that forming (unclosed) GcAV membranes contain punctate structures that are derived from recycling endosomes (REs).[9] Moreover, we found that RAB17-mediated RE recruitment into GcAVs promoted the formation of GcAVs and the elimination of intracellular bacteria, which suggested that the RE functions as a primary membrane source for—and is critical for—autophagosome formation during xenophagy.[9] However, the mechanism of RE fusion with GcAVs remains unclear, and elucidation of this mechanism is crucial for understanding xenophagy.

Specific membrane-fusion events in diverse vesicle-mediated transport pathways are typically regulated by soluble *N*-ethylmaleimide-sensitive factor attachment protein receptor (SNARE) complexes.[10] At the membrane-fusion step, the SNARE complex forms parallel 4-helix bundles comprising the Qa-, Qb-, Qc-, and R-SNAREs. To date, several SNAREs have been shown to function in autophagy in mammals: STX17 (syntaxin 17), SNAP29, VAMP8, VTI1B, and VAMP7 are

CONTACT Ichiro Nakagawa nakagawa.ichiro.7w@kyoto-u.ac.jp Department of Microbiology, Graduate School of Medicine, Kyoto University, Yoshida-konoecho Sakyo-ku, Kyoto 606-8501, Japan.
Supplemental data for this article can be accessed on the publisher's website.

required for lysosome-autophagosome fusion,[11,12] and VAMP8 and VTI1B are also used in GcAV-lysosome fusion.[12] Furthermore, in yeast, Vam3, Vam7, Ykt6, and Vti1 regulate vacuolar fusion.[13,14] With regard to the autophagosome formation process preceding lysosomal fusion, previous studies have reported that VAMP3 mediates heterotypic fusion between ATG9- and ATG16L1-positive vesicles for autophagosome precursor formation,[15] and that yeast Sec22, Ykt6, Tlg2, Sec9, and Sso1 are required for phagophore biogenesis.[16] Thus, identifying the SNARE complex that functions in the RE-autophagosome fusion step is critical for understanding not only xenophagy, but also the fundamental autophagosome formation mechanism in mammals.

In this study, to identify the SNARE complex that is involved in RE-autophagosome fusion during bacterial infection, we examined the subcellular localization of STX-family proteins during GAS infection. We report that STX6 localizes to RE-derived punctate structures on GcAVs and is recruited to GcAVs in response to GAS infection, and that *STX6* knockout impairs RE recruitment to GcAVs and suppresses GcAV formation. Furthermore, we show that VAMP3 and VTI1B function together with STX6 in RE-GcAV fusion.

Results

STX6 localizes to TFRC-positive puncta on GcAVs during GAS infection

To identify the SNARE proteins that mediate RE-GcAV fusion, we examined the localization of EmGFP-fused STX proteins and the autophagosomal marker MAP1LC3B/LC3B during GAS infection in HeLa cells. Out of 11 STX proteins, 5 (STX6, STX10, STX11, STX12, and STX17) were found to clearly colocalize with GAS-surrounding LC3-positive vacuoles (GcAVs) (Fig. S1). We counted the EmGFP-STX-positive GcAVs and determined that EmGFP-STX6 most frequently colocalized with GcAVs (61.5% ± 5.8%) (Fig. 1A). To confirm the GcAV localization of STX6, we examined the subcellular localization of endogenous STX6 during GAS infection. STX6 was detected around GAS and colocalized with GcAVs (Fig. 1B). Furthermore, EmGFP-STX6 showed punctate localization on forming (unclosed) GcAVs (Fig. 1C), and the GcAV colocalization frequency increased with time after infection (Fig. 1D). Next, we examined STX6 colocalization with TFRC, an RE marker, in GAS-infected cells, and found that EmGFP-STX6 clearly colocalized with TFRC on GcAVs (Fig. 1E). To determine whether STX6 preferentially colocalizes with TFRC on GcAVs, we calculated the Pearson's coefficient for colocalization from the GcAV images: STX6 showed significantly higher colocalization with TFRC than with LC3 on GcAVs (Fig. 1F). Furthermore, the signal-intensity plot (Fig. 1G) of STX6 and TFRC together with GcAVs (red line in the figure) revealed coincident signal peaks (orange arrows). These results demonstrate that STX6 colocalizes with TFRC-positive punctate structures on GcAVs. We also performed time-lapse imaging of cells during GAS infection and examined EmGFP-STX6 recruitment into GcAVs. We found that bacteria-containing LC3-positive vacuoles acquired punctate EmGFP-STX6 with time (Fig. 1H), indicating that STX6 is recruited to autophagosomes during GAS infection.

STX6 is involved in RE-GcAV fusion

Because STX6 localized to TFRC-positive puncta on GcAVs, we next knocked down STX6 expression (Fig. 2A) and determined whether STX6 is required for RE-GcAV fusion and GcAV formation: STX6 knockdown led to a reduction in TFRC-positive GcAVs (Fig. 2B and 2C). We also constructed an STX6-knockout HeLa cell line by using the CRISPR/Cas9 genome-editing system (Fig. 2D),[17] and found that in these *STX6*-knockout cells, the TFRC signal was rarely detected on GcAVs (Fig. 2E and 2F). Furthermore, in rescue experiments, FLAG-STX6 expression in the *STX6*-knockout HeLa cells increased RE recruitment to GcAVs (Fig. 2F). To investigate the effects of *STX6* knockout on TF (transferrin) uptake and the endocytosis pathway associated with TFRC, we treated cells with Alexa Fluor 594-labeled human TF and observed internalized TF, and also examined the subcellular localization of TFRC in *STX6*-knockout cells. In our experiments, TF was normally internalized (Fig. S2A), and TFRC frequently colocalized with RAB17 in the perinuclear region and partially overlapped with TGOLN2/TGN46 (TGN marker) in *STX6*-knockout cells (Fig. S2B and S2C). These knockdown and knockout results clearly demonstrate that STX6 functions in RE-GcAV fusion.

RE recruitment to GcAVs involves RAB17 and RABGEF1, and RAB17 inactivation reduces GcAV formation; these findings indicate that REs promote GcAV formation. Thus, to determine whether STX6-mediated RE fusion is involved in GcAV formation, we quantified GcAV formation efficiency in wild-type and *STX6*-knockout HeLa cells: The characteristic large GcAVs were detected only in wild-type cells (Fig. 2G), and significantly fewer *STX6*-knockout cells were GcAV-positive as compared to wild-type cells (Fig. 2H). To ascertain whether or not the defective autophagosome formation in *STX6*-knockout cells affects the viability of intracellular GAS, we determined the number of surviving GAS. Although the number of invaded GAS was not altered, the number of recovered GAS at 4 h after infection significantly increased in *STX6*-knockout cells compared with wild-type cells (Fig. 2I). Collectively, our results suggest that RE-GcAV fusion involves STX6 and that this STX6-mediated fusion facilitates GcAV formation to restrict GAS proliferation in cells.

VAMP3 and VTI1B function together with STX6

Next, we searched for other SNARE proteins that function in the RE-GcAV fusion step together with STX6. Previously, STX6 was found to associate with various SNARE proteins, such as VAMP7, VAMP8, VTI1A, and VTI1B, and was suggested to interact with distinct SNARE partners depending on the cell type examined.[18] Therefore, we screened for the SNARE proteins that localized to TFRC-positive puncta on GcAVs in HeLa cells; our results showed that 6 SNARE proteins colocalized with GcAVs (Fig. S3), and 2 of these proteins, VAMP3 and VTI1B, preferentially colocalized with TFRC on GcAVs, but not with LC3 on GcAVs (Fig. 3A-C). Furthermore, immunoprecipitation analyses revealed that STX6 interacts with VAMP3 and VTI1B during GAS infection (Fig. 3D).

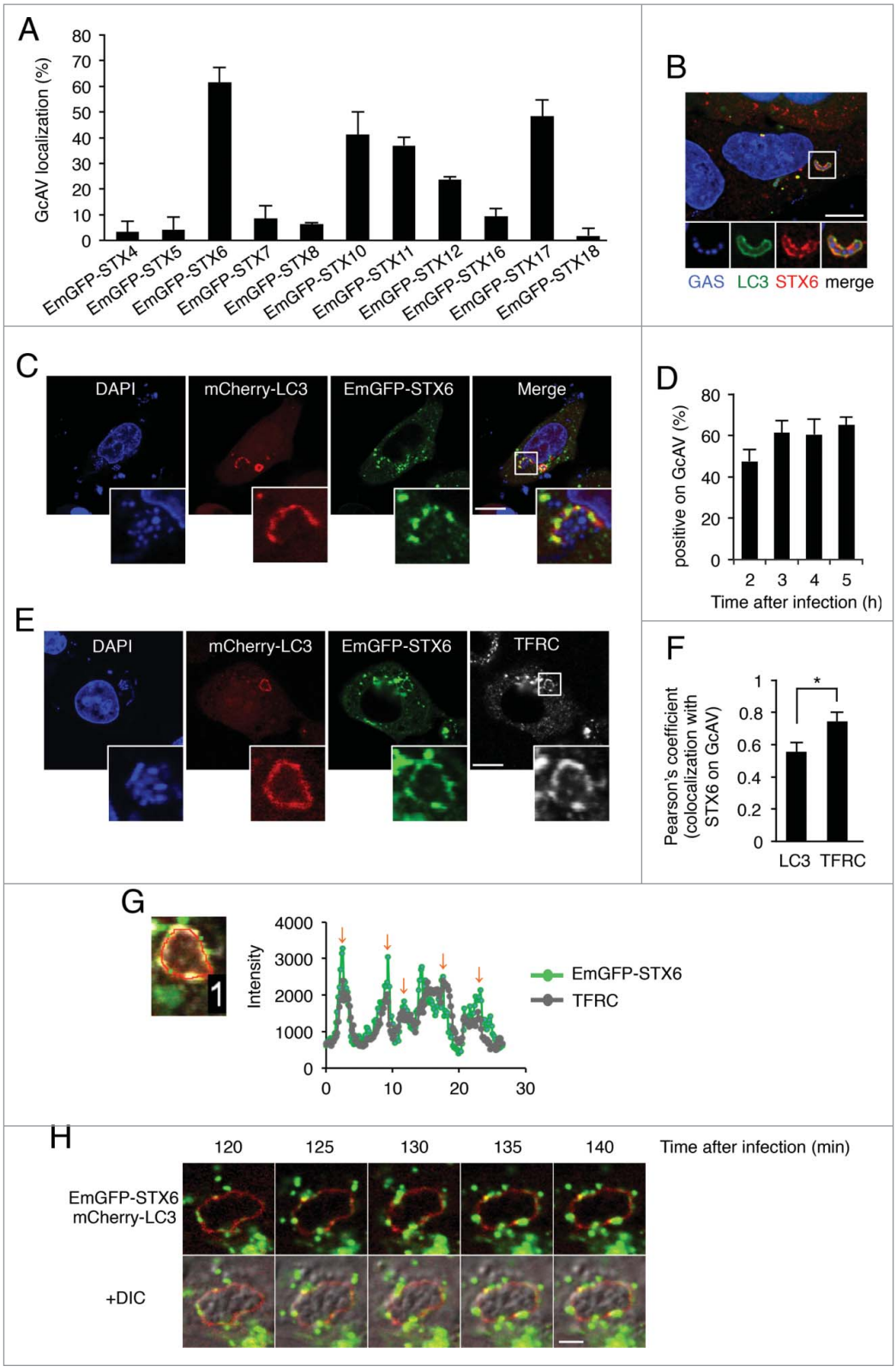

Figure 1. STX6 localizes to TFRC-positive puncta on GcAVs. (A) A screen for STX proteins that colocalize with GcAVs. HeLa cells expressing EmGFP-fused STX proteins and mCherry-fused LC3 (GcAV marker) were infected with GAS for 4 h and fixed. The percentages of EmGFP-STX-positive GcAVs were measured using confocal microscopy. (B) GcAV localization of endogenous STX6. HeLa cells expressing EmGFP-LC3 (green) were infected with GAS for 4 h and stained for STX6 (red). DAPI labels the nuclei and GAS (blue). The insets show high-magnification views of the area outlined in the main merged image. (C) HeLa cells expressing mCherry-LC3 and EmGFP-STX6 were infected with GAS for 2 h. (D) Colocalization of STX6 with GcAVs at different times post-infection. HeLa cells expressing mCherry-LC3 and EmGFP-STX6 were infected with GAS for the indicated times, and the percentages of EmGFP-STX-positive GcAVs were measured using confocal microscopy. (E) Colocalization of STX6 with TFRC and GcAVs. HeLa cells expressing EmGFP-STX6 were infected with GAS for 4 h and then immunostained for TFRC. Scale bars: 10 μm. (F) Pearson's coefficient quantified for STX6-TFRC colocalization on GcAVs. Data represent means $\pm$ SD of $>$10 GcAVs analyzed per condition. (G) Merged image of the GcAV in (E). The graph shows the signal intensities of EmGFP-STX6 and TFRC measured along the red line in the GcAV image. Orange arrows indicate the signal peaks observed in both EmGFP-STX6 and TFRC. (H) Live-cell imaging during GAS infection. HeLa cells expressing EmGFP-STX6 and mCherry-LC3 were infected with GAS for the indicated time points and images were captured by confocal microscopy. Scale bars: 3 μm. DIC, differential interference contrast. Data in (A) and (D) are means $\pm$ SD of 3 independent experiments.

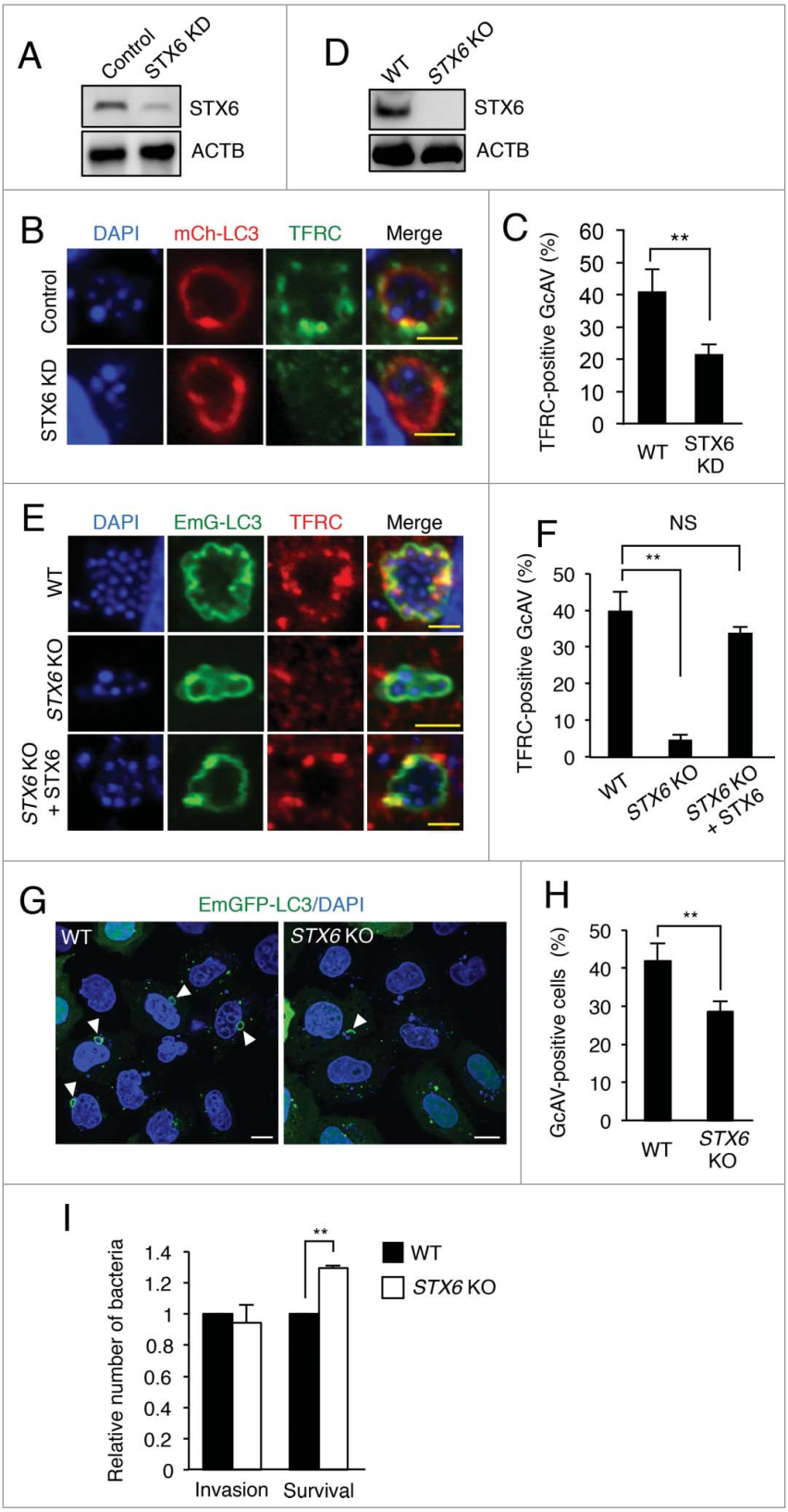

Figure 2. STX6 regulates the fusion between REs and GcAVs. (A) Immunoblotting analysis of STX6-knockdown HeLa cells. (B and C) HeLa cells transfected with control and *STX6 MIR* vectors were infected with GAS for 4 h, fixed, and immunostained for TFRC. DAPI labels the nuclei and GAS. Representative confocal micrographs of GcAVs in control and STX6-knockdown (K_D) HeLa cells (B), and quantification of TFRC-positive GcAVs (C). Yellow scale bars: 3 μm. (D) Immunoblotting analysis of *STX6*-knockout (KO) HeLa cells. (E and F) HeLa wild-type (WT) cells, *STX6*-KO cells, and *STX6*-KO cells expressing FLAG-STX6 were transfected with a plasmid encoding EmGFP-LC3 and infected with GAS for 4 h. Cells were fixed and immunostained for TFRC. Representative confocal micrographs of GcAVs in WT and *STX6*-KO HeLa cells (E), and quantification of TFRC-positive GcAVs (F). (G) and H) HeLa WT and *STX6*-KO cells expressing EmGFP-LC3 were infected with GAS for 4 h. Representative confocal micrographs of the HeLa cells of each type (G), and quantification of GcAV-positive cells (H). (I) HeLa WT and *STX6*-KO cells were infected with GAS for 1, 2, and 4 h. The number of invading and surviving bacteria was measured in the GAS viability assay. Data in (C), (F), (H), and (I) are means ± SD of 3 independent experiments.

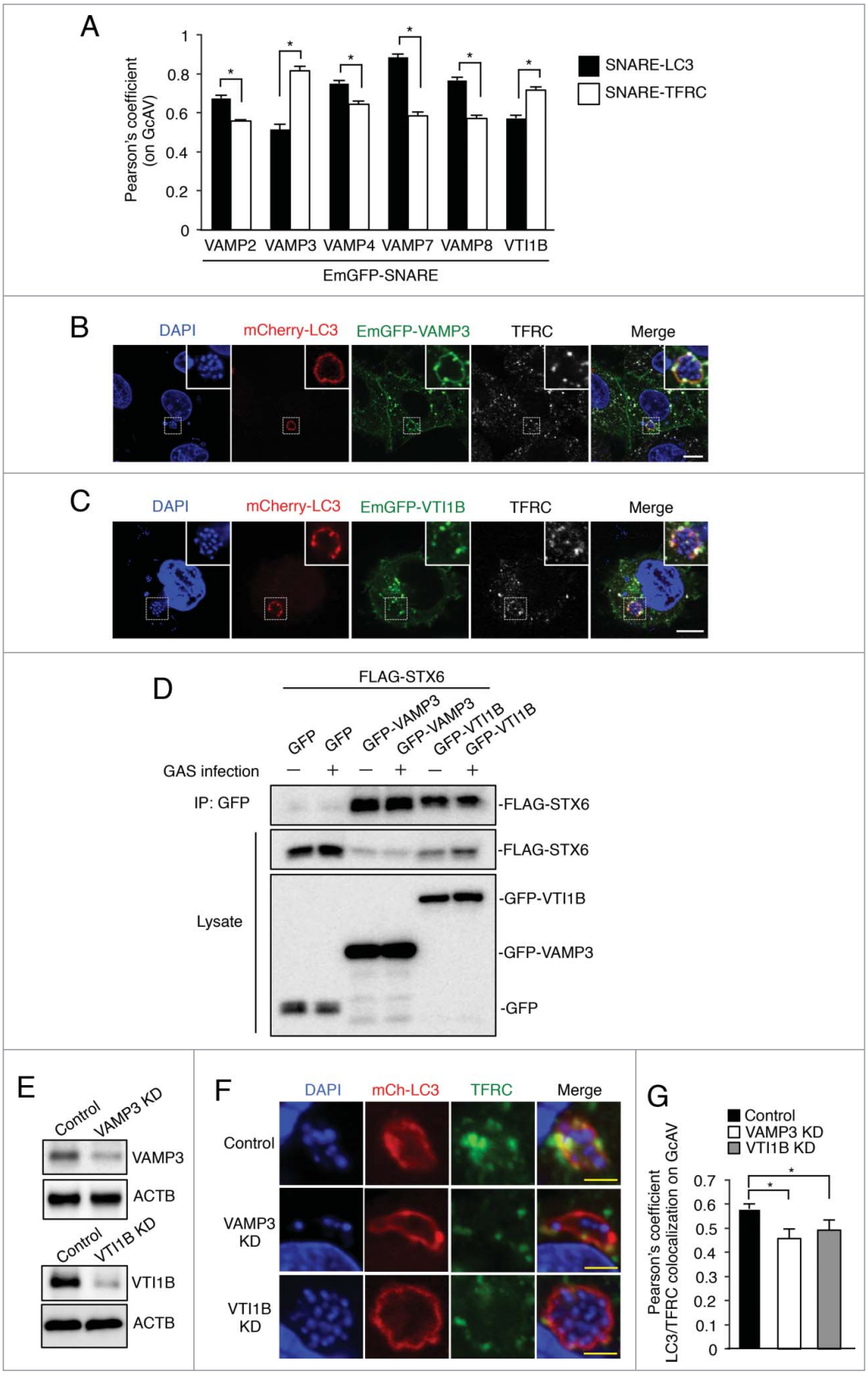

Figure 3. VAMP3 and VTI1B interact with STX6 and promote the fusion between REs and GcAVs. (A–C) HeLa cells expressing EmGFP-SNARE proteins and mCherry-LC3 were infected with GAS for 4 h, fixed, and immunostained for TFRC. Pearson's coefficient quantification of the colocalization of SNARE-LC3 or SNARE-TFRC on GcAVs (A), and representative confocal micrographs of VAMP3- and VTI1B-positive GcAVs (B, C). Data represent means ± SD of >10 GcAVs analyzed per condition. Scale bars: 10 μm. (D) STX6 interacts with VAMP3 and VTI1B. HeLa cells transfected with FLAG-STX6 and EmGFP (GFP), EmGFP-VAMP3, or EmGFP-VTI1B were either not infected or infected with GAS for 4 h, and then subjected to immunoprecipitations with an anti-GFP antibody. The immunoprecipitated proteins and total cell lysates were analyzed by immunoblotting with anti-FLAG and anti-GFP antibodies. (E) Immunoblotting analysis of VAMP3- and VTI1B-knockdown HeLa cells. (F and G) HeLa cells transfected with mCherry-LC3 and MIR-control (Control), -VAMP3 (VAMP3 K_D), or -VTI1B (VTI1B K_D) were infected with GAS for 4 h and then fixed and immunostained for TFRC. Representative confocal micrographs of GcAVs in Control-, VAMP3 K_D, and VTI1B K_D HeLa cells (F), and Pearson's coefficient quantification of the colocalization of LC3-TFRC on GcAVs (G).

To ascertain whether VAMP3 and VTI1B facilitate the fusion between REs and GcAVs, we knocked down the expression of these SNARE proteins (Fig. 3E). VAMP3 knockdown inhibited the Golgi-like perinuclear compartment localization of TF (Fig. S4A). In contrast, VAMP3 and VTI1B knockdown did not affect TF uptake or colocalization between TFRC and RAB17 (Fig. S4A and S4B), suggesting that it did not profoundly affect RAB17-associated TFRC trafficking. However, knockdown of either VAMP3 or VTI1B significantly reduced the colocalization of TFRC and GcAVs (Fig. 3F and 3G). Collectively, these results suggest that VAMP3 and VTI1B cooperate with STX6 in the RE-GcAV fusion process.

The H2 SNARE domain of STX6 is required for punctate localization on GcAVs and interaction with VAMP3 and VTI1B

We next sought to identify the domains of STX6 that are responsible for its localization to GcAVs and the TFRC-positive punctate structures on GcAVs. The *STX6* gene encodes a protein containing 255 amino acids, and the C-terminal 20 amino acids of STX6 are hydrophobic and form a transmembrane (TM) domain.[18] STX6 further contains 2 coiled-coil domains—H1 and H2—that have been implicated in mediating protein interactions,[18] and one tyrosine-based sorting motif (YGRL, residues 140–143). We constructed STX6 deletion mutants lacking the aforementioned domains (Fig. 4A) and quantified their GcAV colocalization in HeLa cells. Deletion of the TM domain suppressed STX6 targeting to all membranes, including GcAVs (Fig. 4B and 4C), which suggests that the TM domain is necessary for GcAV localization of STX6. Moreover, although STX6 166–255 and ΔYGRL mutants appeared to retain their intracellular membrane localization, they also failed to localize to GcAVs (Fig. 4B and 4C). These results suggest that the YGRL sorting motif is required for GcAV targeting. Intriguingly, EmGFP-STX6 ΔH2 was detected on GcAVs but did not display the punctate localization, and this mutant showed higher colocalization with LC3 than did wild-type STX6 (Fig. 4B and 4C). Additionally, the signal peaks of EmGFP-STX6 ΔH2 did not coincide with those of TFRC on GcAVs (Fig. 4D). These results suggest that the H2 domain is required for the TFRC-positive punctate localization of STX6 on GcAVs.

The H2 domain is also known as the SNARE core domain, and thus we performed immunoprecipitation assays by using the STX6 deletion mutants to examine the domain's role in STX6 interactions: VAMP3 precipitated with STX6 wild-type and ΔH1 but not ΔH2 (Fig. 4E), which suggested that the STX6 H2 domain interacts with VAMP3. Similarly, STX6 ΔH2 did not interact with VTI1B (Fig. 4E). To determine whether the H2 domain and YGRL motif are required for GcAV formation, we performed rescue experiments using these deletion constructs. Expression of full-length STX6 recovered GcAV formation efficiency in *STX6*-knockout cells, and this recovery was not observed in ΔH2 or ΔYGRL mutants (Fig. 4F). Taken together, our findings suggest that STX6 is recruited to GcAVs by the YGRL sorting motif and is localized in the membrane through its TM domain, and further that STX6 exhibits a punctate localization and interacts with other SNARE proteins through the H2 SNARE domain.

RABGEF1 is required for STX6-mediated RE-GcAV fusion

We previously reported that RAB17 and RABGEF1 regulate RE recruitment into GcAVs and GcAV formation and thereby facilitate xenophagy.[9] In the present study, we investigated whether the STX6-VAMP3-VTI1B complex colocalizes with RAB17-positive vesicles. EmGFP-STX6 and -VAMP3 colocalized with mCherry-RAB17 in the perinuclear region and in many vesicles; however, VTI1B only colocalized with RAB17 in the perinuclear region (Fig. S5). Thus, to determine whether RAB17-RABGEF1 and the STX6-VAMP3-VTI1B complex function in the same pathway during GcAV formation, we generated a *RABGEF1*-knockout HeLa cell line (Fig. 5A) and analyzed the involvement of the STX6-VAMP3-VTI1B complex. First, we examined the colocalization of LC3 and TFRC during GAS infection, and found that the colocalization between GcAVs and TFRC was decreased in *RABGEF1*-knockout cells (Fig. 5B and 5C); furthermore, GcAV formation efficiency was also reduced in the knockout cells (Fig. 5D). Expression of RABGEF1 increased the numbers of both TFRC-positive GcAV and GcAV-positive cells among *RABGEF1*-knockout cells (Fig. 5B-5D), confirming that RABGEF1 facilitates RE-GcAV fusion and GcAV formation. These results agreed with the findings of our previous study.[9] Next, we analyzed the effects of *RABGEF1* knockout on the GcAV localization of STX6, VAMP3, and VTI1B. Whereas EmGFP-STX6 and -VTI1B were detected on GcAVs at similar levels in wild-type and *RABGEF1*-knockout cells, EmGFP-VAMP3-positive GcAVs were rarely observed in the knockout cells (Fig. 5E). Quantification of the colocalization between EmGFP-SNAREs and GcAVs revealed that the colocalization of VAMP3 with GcAVs was substantially lower in *RABGEF1*-knockout cells than in control cells (Fig. 5F). These data suggest that VAMP3 recruitment to GcAVs is regulated by RABGEF1.

Furthermore, to ascertain whether STX6-VAMP3-VTI1B interactions are also regulated by RABGEF1, we performed immunoprecipitations with the *RABGEF1*-knockout cells. Although the interaction between STX6 and VTI1B was almost equal in control and knockout cells, the association between STX6 and VAMP3 was substantially decreased in *RABGEF1*-knockout cells (Fig. 5G and 5H), which indicates that RABGEF1 is required for the interaction between STX6 and VAMP3. Collectively, these results suggest that VAMP3 is recruited to GcAVs through a RABGEF1-mediated pathway and forms a complex with STX6, thus mediating RE-GcAV fusion.

STX6 but not RABGEF1 is involved in starvation-induced autophagosome formation

Last, we examined the involvement of STX6 and RABGEF1 in autophagy during starvation. LC3-II levels increased under starvation or treatment with protease inhibitors (E64d and pepstatin A) in wild-type cells; however, *STX6* knockout suppressed LC3-II accumulation under starvation and protease inhibitor-treated conditions (Fig. 6A and 6B). This finding suggests that autophagosome formation was impaired. In contrast, the LC3-II level increased in response to starvation in *RABGEF1*-knockout cells (Fig. 6C and 6D), suggesting that RABGEF1 is dispensable for starvation-induced autophagosome formation.

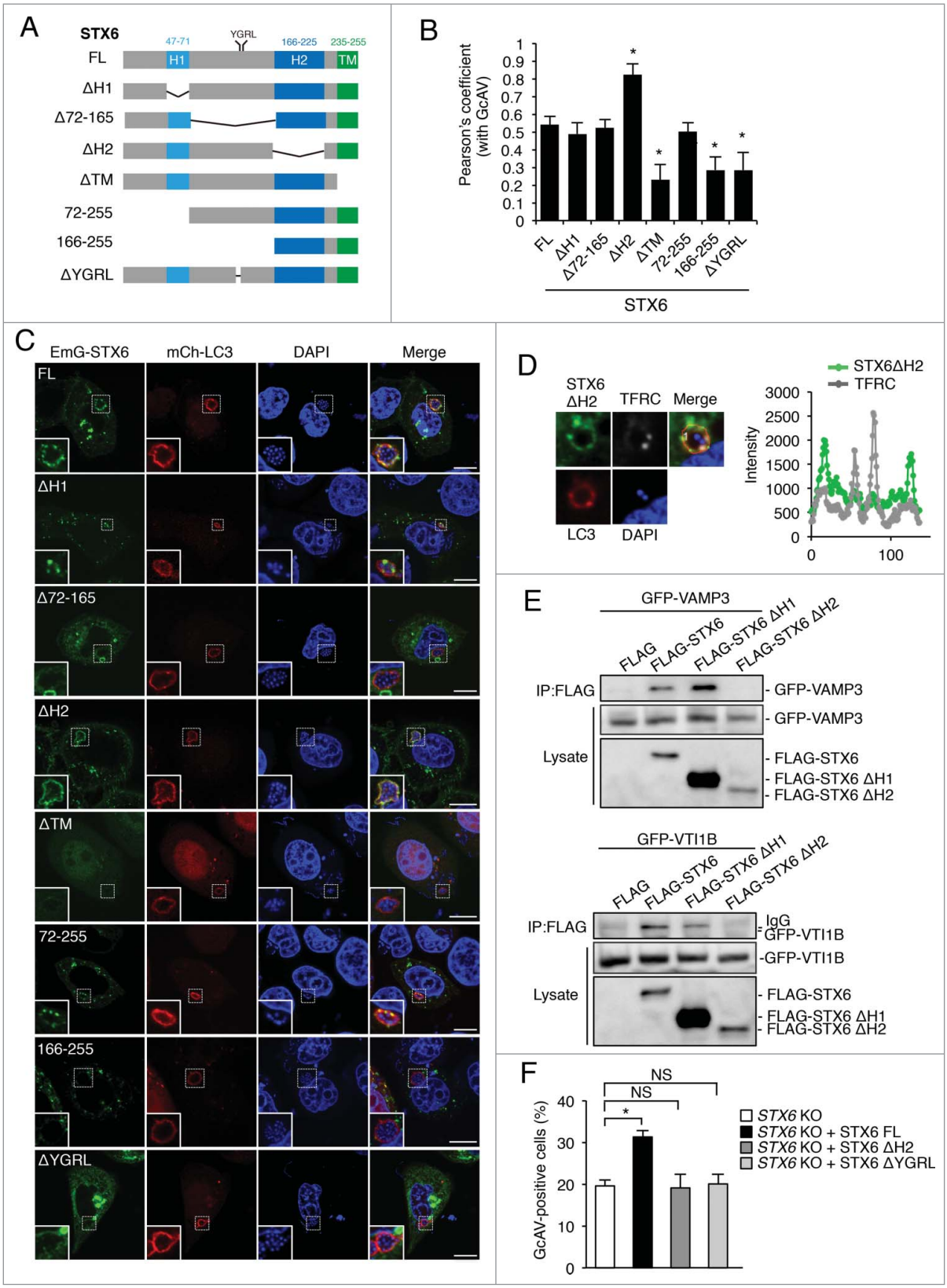

Figure 4. STX6 regions required for punctate localization on GcAVs, interaction with VAMP3 and VTI1B, and recruitment to GcAVs. (A) Schematic map showing STX6 domain organization and deletion constructs used in this study. (B and C) HeLa cells transfected with EmGFP-STX6 constructs and mCherry-LC3 were infected with GAS for 4 h. Pearson's coefficient quantification of the colocalization of STX6 constructs with LC3 on GcAVs (B), and representative confocal micrographs of GcAVs (C). Scale bars: 10 μm. (D) HeLa cells expressing EmGFP-STX6 ΔH2 and mCherry-LC3 were infected with GAS for 4 h and then immunostained for TFRC. The graph shows the signal intensities of EmGFP-STX6 and TFRC measured along the red line in the merged image. (E) The STX6 H2 domain is required for interaction with VAMP3 and VTI1B. HeLa cells transfected with EmGFP-VAMP3 or -VTI1B and FLAG, FLAG-STX6, FLAG-STX6 ΔH1, or FLAG-STX6 ΔH2 were subjected to immunoprecipitations with an anti-FLAG antibody. The immunoprecipitated proteins and total cell lysates were analyzed by immunoblotting with anti-FLAG and anti-GFP antibodies. (F) HeLa *STX6*-KO cells expressing EmGFP-LC3 and FLAG-control, -STX6 FL, -STX6 ΔH2, or -STX6 ΔYGRL were infected with GAS for 4 h. The percentages of GcAV-positive cells were quantified using confocal microscopy. Data are the mean ± SD of 3 independent experiments.

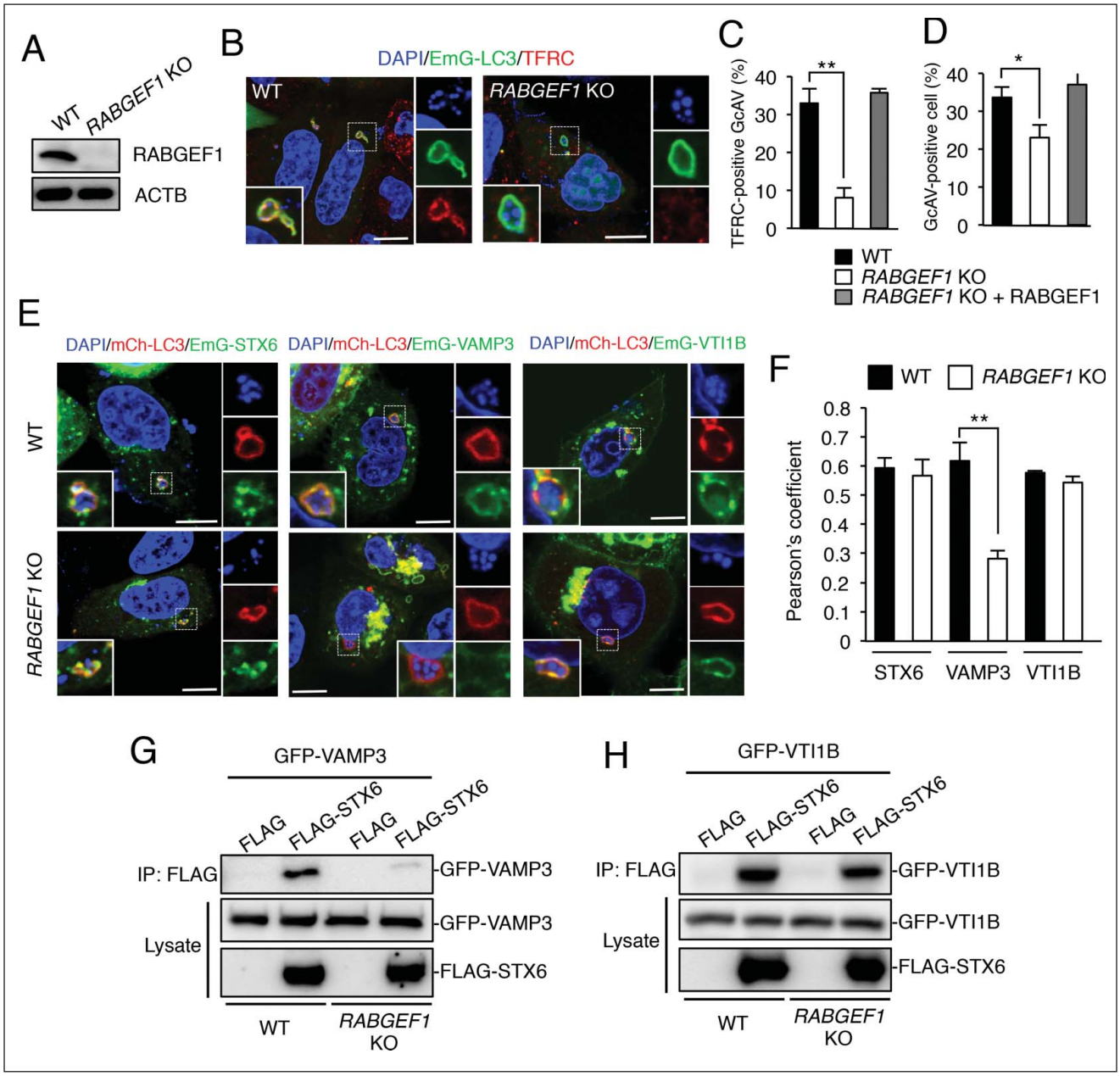

Figure 5. RABGEF1 is critical for the STX6-VAMP3 interaction and RE-GcAV fusion required to promote xenophagy. (A) Immunoblotting analysis of *STX6*-KO HeLa cells. (B–D) Involvement of RABGEF1 in RE recruitment and GcAV formation. HeLa WT and *RABGEF1*-KO cells were transfected with plasmids encoding EmGFP-LC3 and FLAG-RABGEF1, infected with GAS for 4 h, and then fixed and immunostained for TFRC. Representative confocal micrographs of each cell type (B), and quantification of TFRC-positive GcAVs (C) and GcAV-positive cells (D). (E and F) Effects of *RABGEF1* KO on GcAV localization of STX6, VAMP3, and VTI1B. HeLa WT and *RABGEF1*-KO cells were transfected with plasmids encoding mCherry-LC3 and EmGFP-STX6, -VAMP3, or -VTI1B, and then infected with GAS for 4 h. Representative confocal micrographs of each cell type (E), and Pearson's coefficient quantification of colocalization on GcAVs (F). (G and H) RABGEF1 is required for the interaction between STX6 and VAMP3. HeLa WT and *RABGEF1*-KO cells were transfected with EmGFP-VAMP3 (G) or -VTI1B (H) and FLAG or FLAG-STX6, and subjected to immunoprecipitations with the anti-FLAG antibody. The immunoprecipitated proteins and total cell lysates were analyzed by immunoblotting with anti-FLAG and anti-GFP antibodies.

In wild-type cells, the number of GFP-LC3 puncta increased during starvation (Fig. 6E and 6F). The number of GFP-LC3 puncta also increased slightly even in *STX6*-knockout cells; however, the number was still significantly lower than that in wild-type cells (Fig. 6E and 6F). Taken together, these findings suggest that STX6 but not RABGEF1 is involved in autophagosome formation under starvation conditions.

Discussion

In this study, we showed that STX6 regulates the fusion between autophagosomes and REs and thereby promotes autophagosome biogenesis during xenophagy. STX6 targets the GAS-capturing, forming (unclosed) GcAVs through its tyrosine-based sorting motif and localizes to RE-derived punctate structures on GcAVs. VTI1B and VAMP3 also localize to this punctate structure, and the recruitment of VAMP3 depends on a RABGEF1-mediated RE-GcAV fusion pathway. Notably, the results of knockdown and knockout analysis showed that the STX6-VAMP3-VTI1B complex is required for the GcAV-RE fusion and GcAV formation necessary for xenophagy.

STX6 is widely recognized to participate in various fusion events.[18] However, this is the first report of STX6 involvement in autophagy. STX6 mainly localizes to the *trans*-Golgi network

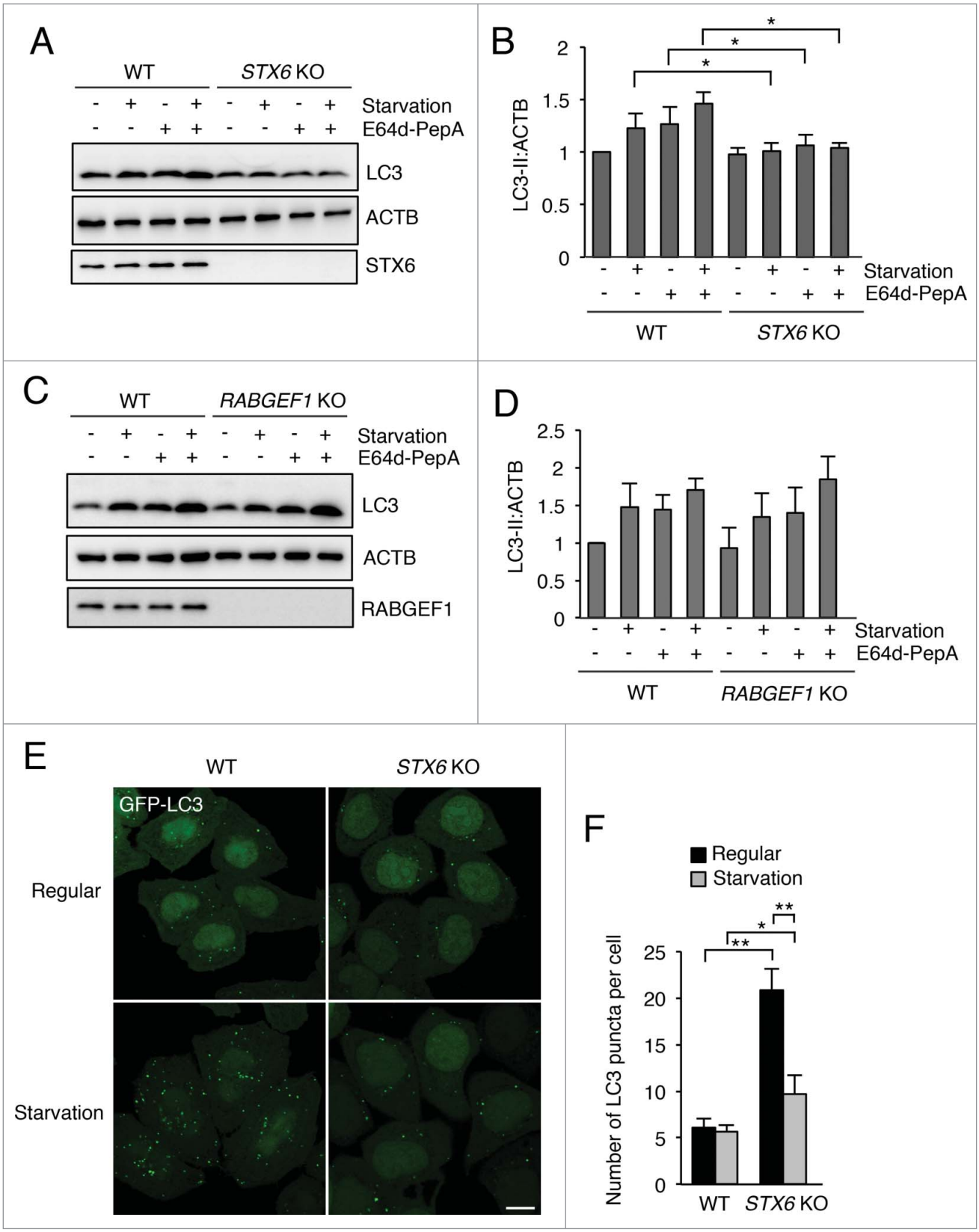

Figure 6. STX6 but not RABGEF1 is involved in starvation-induced autophagosome formation. (A and B) WT and *STX6* KO cells were cultured in regular or starvation medium for 2 h with or without E64d and pepstatin A, and analyzed by immunoblotting (A). The LC3-II level was quantified and normalized to that of ACTB (B). (C and D) WT and *RABGEF1* KO cells were cultured in regular or starvation medium for 2 h with or without E64d and pepstatin A, and analyzed by immunoblotting (C). The LC3-II level was quantified and normalized to that of ACTB (D). HeLa WT and *STX6* KO cells stably expressing EGFP-LC3 were cultured in regular or starvation medium for 2 h. Confocal micrographs (E) and quantification of the number of LC3 puncta (F). Data in (B), (D), and (F) are the mean ± SD of 3 independent experiments.

(TGN) and endosomal structures, and is suggested to regulate SLC2A4/GLUT4 trafficking,[19] the secretory pathway,[20] caveolar endocytosis,[21] and endosome-TGN retrograde transport.[22] TFRC-positive REs are also incorporated into starvation-induced autophagosomes and facilitate autophagosome formation, and their trafficking is regulated by TBC1D14 and RAB11.[23] However, the fusion of REs with GcAVs is mediated by RAB17 rather than RAB11,[9] and thus the SNARE machinery involved in the RE-autophagosome fusion step might also differ between canonical autophagy and xenophagy.

We revealed the GcAV localization of STX6 in this study and identified the STX6 domains required for the protein's targeting to and punctate localization on GcAVs. Because the number of STX6-positive GcAVs increased with time, STX6 is likely acquired by GcAVs and not initially contained in GcAV precursors. Notably, deletion of the tyrosine-based motif YRGL in STX6 prevented the recruitment of STX6 to GcAVs (Fig. 4B and 4C). The YGRL motif of STX6 functions in the return to the *trans*-Golgi from the plasma membrane,[24] and it is also required for targeting to the *Chlamydia* inclusion membrane.[25,26] Kabeiseman et al. suggested that deletion or alteration of the YGRL region does not markedly affect the protein interactions of STX6, but reduces the interaction with lipids such as phosphatidylinositol 3-phosphate, phosphatidylinositol 4-phosphate, and phosphatidylinositol 5-phosphate.[26] Therefore, although it is not yet clear whether STX6 is recruited to GcAVs through lipid interactions, further investigation of the lipid contents of GcAVs should help enhance our understanding of STX6 recruitment.

We found that STX6 forms a complex with VTI1B and VAMP3 and that this complex defends cells through autophagy. Interestingly, STX6 and VTI1B have been reported to function as a part of the Q-SNARE complex (STX6-VAMP7-VTI1B) on the TGN together with the R-SNARE VAMP3 and thereby regulate TNF/TNFα trafficking in macrophages.[27] Moreover, the STX6-VTI1B-VAMP3 complex has been reported to regulate the IL6 secretion pathway through REs in macrophages.[28] Because STX6 is suggested to change its SNARE partners and thus specifically regulate several different fusion events, the STX6-VTI1B-VAMP3 complex could be activated in response to pathogenic infection. Intriguingly, STX6 is a cholesterol-binding protein,[29] and alteration of the cholesterol level at the TGN/endosome boundary causes STX6 accumulation on VAMP3-positive REs.[30] Bacterial pathogens carry secreted toxins that interact with cholesterol and affect its intracellular balance,[31,32] and streptolysion O, a cytolysin secreted by GAS, also interacts with cholesterol molecules in target bilayers and could affect cholesterol dynamics.[33] This raises the possibility that the STX6-VAMP3-VTI1B complex is activated in response to changes in cholesterol levels during bacterial infection.

VTI1B has been reported to be involved in the fusion between GcAVs and lysosomes, which suggests that VTI1B regulates multiple steps of the GcAV formation process. Furuta et al.[12] reported that VTI1B is recruited to GcAVs before lysosomal fusion, and our results also showed that VTI1B colocalized with forming (unclosed) GcAVs (Fig. 3C). However, VTI1B mainly localizes in the TGN and endosomes[34] and is recruited to GcAVs even in *RABGEF1*-knockout cells; thus, we suggest that VTI1B targets GcAVs through a pathway distinct from that used by VAMP3.

Although this finding is slightly out of the scope of the present study, we found that STX6 is required for autophagosome formation under starvation conditions (Fig. 6A, 6B, 6E and 6F). Importantly, RABGEF1 was dispensable for starvation-induced autophagosome formation (Fig. 6C and 6D), in agreement with our previous data. Because STX6-mediated RE fusion involves RABGEF1, STX6 might be involved in canonical autophagy through a mechanism different from that involved in xenophagy. Zhang et al. reported that OGT (O-linked N-acetylglucosamine [GlcNAc] transferase) modifies the SNARE protein SNAP29 in a nutrient-dependent manner and implied that the STX6-SNAP29 complex is involved in autophagy induction.[35,36] Considering our results regarding starvation-induced autophagy, STX6 may be an essential regulator in canonical autophagy.

In this study, we showed that GcAV localization was exhibited by 11 SNAREs (EmGFP-fused STX6, STX10, STX11, STX12, STX17, VAMP2, VAMP3, VAMP4, VAMP7, VAMP8, and VTI1B), but roles in GcAV formation have been identified for only 5 of these SNAREs; we have described the function of STX6. Our finding that several SNAREs localize on GcAVs suggests the involvement of multiple organelle-derived vesicles in GcAV formation, but the functions of other SNAREs in xenophagy remain unclear. Additional studies on SNAREs will not only help reveal the molecular mechanism of GcAV formation, but also enhance our understanding of canonical autophagy.

Materials and methods

Cell culture and transfection

HeLa cells were maintained in Dulbecco's modified Eagle's medium (Nacalai Tesque, 18459-64) supplemented with 10% fetal bovine serum (Gibco, 26140079) and 50 μg/mL gentamicin (Nacalai Tesque, 11980-14) in a 5% CO_2 incubator at 37°C. The transfection reagents used were polyethylenimine (Polysciences, 23966-2) and Lipofectamine 3000 (Invitrogen Corporation, L3000001).

Bacterial strain

GAS strain JRS4 ($M6^+$ $F1^+$) was grown in Todd-Hewitt broth (BD Diagnostic Systems, 249240) supplemented with 0.2% yeast extract (THY) as described previously.[6]

Antibodies and other reagents

The following primary antibodies were used: rabbit monoclonal anti-STX6/syntaxin 6 (C34B2; 2869), rabbit polyclonal anti-VAMP3 (13640), rabbit monoclonal anti-ACTB/β-actin (D6A8; 8457), and rabbit monoclonal anti-RABGEF1/Rabex5 (D21F12; 7622), from Cell Signaling Technology; rabbit polyclonal anti-VTI1B (Proteintech Group, 14495-1-AP); mouse monoclonal anti-TFRC/CD71 (OX26; Santa Cruz Biotechnology, sc-53059); mouse monoclonal anti-FLAG (M2; Sigma-Aldrich, A2220); and mouse monoclonal anti-GFP (GF200; Nacalai Tesque, 04363-24). The secondary antibodies used were the following: for immunoblotting, HRP-conjugated anti-rabbit and anti-mouse IgG (Jackson ImmunoResearch Laboratories, 111-035-144 and 115-035-003, respectively); for immunostaining, Cy5 goat anti-rabbit IgG (Jackson ImmunoResearch Laboratories, 711-175-152), and anti-mouse

or anti-rabbit IgG conjugated with Alexa Fluor 488 or 594 (Invitrogen Corporation, A-11001, A-11008, A-11032, and A-21442). E64d (Enzo Life Sciences, BML-PI107-0001) and pepstatin A (Nacalai Tesque, 26305-03-3) were used at 10 μg/mL and 30 μg/mL, respectively.

Plasmids

Human SNARE cDNAs were PCR-amplified from HeLa, KYSE, and HEK293T cell total mRNAs and cloned into pcDNA-6.2/N-EmGFP-DEST (N-terminal tagged; Invitrogen Corporation, V35620), pcDNA-6.2/N-3xFLAG-DEST (N-terminal tagged), and pcDNA-6.2/N-mCherry-DEST (N-terminal tagged) by using Gateway cloning technology as described previously.[8] pcDNA-6.2/N-3xFLAG-DEST and pcDNA-6.2/N-mCherry-DEST vectors were made by replacement from pcDNA-6.2-N-EmGFP to the 3xFLAG corresponding oligonucleotide or mCherry gene fragment (kindly provided from Dr. Tsien) for compatible with the Gateway system, respectively. A BLOCK-iT Pol II miR-RNAi expression vector kit (Invitrogen Corporation, K493500) was used to knock down STX6, VAMP3, and VTI1B expression. We used the following targeting sequences: *STX6*, 5′-TACAAGTACTCGGCAAGTTGT-3′; *VAMP3*, 5′-TGGCAGTAATCGAAGACTTCA-3′; and *VTI1B*, 5′-GATGTCTAAGCTTCGAAACTA-3′. The miRNA double-strand sequences were ligated to pcDNA-6.2-GW/miR, as per supplier instructions; pcDNA6.2-GW/miR-neg was used as the miRNA control. These plasmids were transfected into HeLa cells as described above. Knockdowns were confirmed through immunoblotting.

Generation of knockout lines by using CRISPR/Cas9 gene editing

We used the CRISPR/Cas9 system to generate *STX6*- and *RABGEF1*-knockout cell lines, as described previously.[37] Briefly, CRISPR guide RNAs (gRNAs) were selected that targeted an exon common to all splicing variants of the gene of interest (*STX6*: ATGTCAACTTCATCTGTGC; *RABGEF1*: TCTCATCATCAGTAGTTTC). For CRISPR/Cas9 gene editing, HeLa cells were transfected with the gRNA-hyg vector containing CRISPR target sequences and hCAS9[17] (Addgene, 41815; George Church Lab). After the transfection step, untransfected cells were removed through selection with 300 μg/mL hygromycin B and 750 μg/mL geneticin (G418) (both from Nacalai Tesque, 09287-84 and 16513-26, respectively). Single colonies were expanded and the depletion of the targeted gene product was confirmed through immunoblotting. As a secondary screen of certain knockout lines, genomic DNA was isolated from cells and the genomic regions of interest were amplified using PCR. The targeted genomic regions of the knockout lines were also sequenced to confirm the presence of frameshifting indels in the genes of interest.

Generation of cell lines with stable transgene expression

Cell lines with stable transgene expression were generated by retroviral infection as previously described. Based on pLenti6/V5-DEST, the virus was produced using the ViraPower lentiviral expression system (Invitrogen Corporation, K4960-00) according to the manufacturer's protocol. Briefly, 293 FT cells were cotransfected with pLenti-EmGFP-LC3 and the mixture of packaging plasmids (Invitrogen Corporation, K4975-00) using Lipofectamine 3000, and then cultured for 48 h. The viral supernatant was collected and used to infect HeLa cells. After 24 h, uninfected cells were removed by selection on 5 μg/mL blasticidin (Invitrogen Corporation, A1113903).

Bacterial infection

Cells were infected with GAS as described previously.[6] Briefly, bacteria were incubated with cell cultures for 1 h at a multiplicity of infection of 100 in the absence of antibiotics. The infected cells were washed with phosphate-buffered saline (PBS; 137 mM NaCl, 2.7 mM KCl, 8.1 mM Na_2HPO_4, 1.47 mM KH_2PO_4, pH 7.4) and the antibiotic gentamicin (100 μg/mL) was added for an appropriate period to kill extracellular bacteria.

Fluorescence microscopy and image analyses

For confocal microscopy analysis, cells were cultured on 12-mm-diameter glass coverslips in 24-well culture plates. The cells were placed on a glass-bottom dish to facilitate time-lapse imaging. For immunostaining, cells were washed with PBS, fixed with 4% paraformaldehyde in PBS for 15 min, permeabilized with 0.1% Triton X-100 (Nacalai Tesque, 35501-15) in PBS for 10 min, washed again with PBS, and then incubated in skim milk blocking buffer (5% skim milk, 2.5% goat serum [Sigma-Aldrich, G9023], 2.5% donkey serum [Millipore, S30], 0.1% gelatin [BD Diagnostic Systems, No. 214340] in PBS) or BSA blocking buffer (2% BSA [Sigma-Aldrich, A4503] in PBS) at room temperature for 1 h. Subsequently, the cells were incubated (room temperature, 1 h) with primary antibodies diluted with blocking solution, washed with PBS, and then probed with secondary antibodies. Bacterial and cellular DNAs were stained with 4′,6-diamidino-2-phenylindole (DAPI; Dojindo, D523). All fluorescence micrographs shown here are confocal images acquired using an FV1000 laser-scanning microscope (Olympus). For quantitative analysis, cell images were captured at random using the confocal microscope, and then colocalization was determined by calculating the Pearson's coefficient after tracing individual cells by using ImageJ software (National Institutes of Health).

TF uptake

Cells were incubated with 5 μg/mL Alexa Fluor 594-labeled human TF/transferrin (Invitrogen Corporation, T13343) for 1 h at 37°C. Cells were washed with PBS and fixed, and the fluorescence intensity per cell was measured by confocal microscopy and ImageJ software. More than 10 randomly selected images were analyzed in each condition.

Bacterial viability assay

HeLa cells (4×10^4 cells/well) were cultured in 24-well culture plates and infected as described in "Bacterial infection." After an appropriate incubation period, cells were lysed in sterile distilled water and serial dilutions of the lysates were plated on THY agar plates. The number of invaded and surviving GAS was determined through colony counting. The invasion data

are presented as the ratio of total intracellular GAS at 2 h to total adhered and internalized GAS at 1 h, and the survival data are presented as the ratio of intracellular live GAS at 4 h to total intracellular GAS at 2 h.

Immunoprecipitation

For immunoprecipitation, cells were harvested, washed with PBS, and lysed in a lysis buffer (10 mM Tris-HCl, pH 7.4, 150 mM NaCl, 10 mM $MgCl_2$, 1 mM EDTA, 1% Triton X-100) containing a proteinase inhibitor cocktail (Nacalai Tesque, 25955-11) for 30 min on ice. The lysates were centrifuged and the obtained supernatants were pre-cleared by incubating with protein A Sepharose 4B (GE Healthcare Life Sciences, 17-1279-03) for 30 min at 4°C. After brief centrifugation (600 × g, 1 min), the supernatants were reacted with anti-FLAG or anti-GFP antibodies for 2 h at 4°C, and then protein A Sepharose beads were added and allowed to react (with rotation) for 1 h at 4°C. The immunoprecipitates were collected by briefly centrifuging the mixtures, washed 5 times with lysis buffer, and analyzed through immunoblotting.

Statistical analysis

Colocalization and GcAV formation were quantified through direct visualization performed using confocal microscopy. Unless indicated otherwise, at least 50 GcAVs or 200 GAS-infected cells were counted per condition in each experiment, and at least 3 independent experiments were performed for each trial. Values, including those displayed in graphs, are means ± SD. Statistical analysis was performed using a 2-tailed Student *t* test. $P < 0.05$ was considered to indicate statistical significance; significance is marked as * for $P < 0.05$, ** for $P < 0.01$, *** for $P < 0.001$, and NS for not significant.

Abbreviations

BSA	bovine serum albumin
DAPI	4′,6-diamidino-2-phenylindole
EmGFP	emerald green fluorescent protein
GAS	Group A *Streptococcus*
GcAV	GAS-containing autophagosome-like vacuole
MAP1LC3B/LC3B	microtubule-associated protein 1 light chain 3 β (a mammalian ortholog of yeast Atg8)
RE	recycling endosome
SNARE	soluble *N*-ethylmaleimide-sensitive factor attachment protein receptor
TGN	*trans*-Golgi network
TM	transmembrane.

Disclosure of potential conflicts of interest

No potential conflicts of interest were disclosed.

Funding

This research was supported in part by Grants-in-Aid for Scientific Research (25293370, 15K15130, 26462776, 16H05188), the funding program for Next Generation World-Leading Researchers (LS041) (I.N.), and the Daiichi Sankyo Foundation of Life Science (I.N.).

References

[1] Mizushima N, Komatsu M. Autophagy: renovation of cells and tissues. Cell 2011; 147:728-41; PMID:22078875; http://dx.doi.org/10.1016/j.cell.2011.10.026

[2] Tooze SA, Yoshimori T. The origin of the autophagosomal membrane. Nat Cell Biol 2010; 12:831-5; PMID:20811355; http://dx.doi.org/10.1038/ncb0910-831

[3] Levine B. Eating oneself and uninvited guests: autophagy-related pathways in cellular defense. Cell 2005; 120:159-62; PMID:15680321

[4] Kuballa P, Nolte WM, Castoreno AB, Xavier RJ. Autophagy and the immune system. Annu Rev Immunol 2012; 30:611-46; PMID:22449030; http://dx.doi.org/10.1146/annurev-immunol-020711-074948

[5] Deretic V, Levine B. Autophagy, immunity, and microbial adaptations. Cell Host Microbe 2009; 5:527-49; PMID:19527881; http://dx.doi.org/10.1016/j.chom.2009.05.016

[6] Nakagawa I, Amano A, Mizushima N, Yamamoto A, Yamaguchi H, Kamimoto T, Nara A, Funao J, Nakata M, Tsuda K, et al. Autophagy defends cells against invading group A Streptococcus. Science 2004; 306:1037-40; PMID:15528445; http://dx.doi.org/10.1126/science.1103966

[7] Yamaguchi H, Nakagawa I, Yamamoto A, Amano A, Noda T, Yoshimori T. An initial step of GAS-containing autophagosome-like vacuoles formation requires Rab7. PLoS Pathog 2009; 5:e1000670; PMID:19956673; http://dx.doi.org/10.1371/journal.ppat.1000670

[8] Nozawa T, Aikawa C, Goda A, Maruyama F, Hamada S, Nakagawa I. The small GTPases Rab9A and Rab23 function at distinct steps in autophagy during Group A Streptococcus infection. Cell Microbiol 2012; 14:1149-65; PMID:22452336; http://dx.doi.org/10.1111/j.1462-5822.2012.01792.x

[9] Haobam B, Nozawa T, Minowa-Nozawa A, Tanaka M, Oda S, Watanabe T, Aikawa C, Maruyama F, Nakagawa I. Rab17-mediated recycling endosomes contribute to autophagosome formation in response to Group A Streptococcus invasion. Cell Microbiol 2014; 16:1806-21; PMID:25052408; http://dx.doi.org/10.1111/cmi.12329

[10] Hong W. SNAREs and traffic. Biochim Biophys Acta 2005; 1744:493-517; PMID:16038056; http://dx.doi.org/10.1016/j.bbamcr.2005.03.014

[11] Itakura E, Kishi-Itakura C, Mizushima N. The hairpin-type tail-anchored SNARE syntaxin 17 targets to autophagosomes for fusion with endosomes/lysosomes. Cell 2012; 151:1256-69; PMID:23217709; http://dx.doi.org/10.1016/j.cell.2012.11.001

[12] Furuta N, Fujita N, Noda T, Yoshimori T, Amano A. Combinational soluble N-ethylmaleimide-sensitive factor attachment protein receptor proteins VAMP8 and Vti1b mediate fusion of antimicrobial and canonical autophagosomes with lysosomes. Mol Biol Cell 2010; 21:1001-10; PMID:20089838; http://dx.doi.org/10.1091/mbc.E09-08-0693

[13] Darsow T, Rieder SE, Emr SD. A multispecificity syntaxin homologue, Vam3p, essential for autophagic and biosynthetic protein transport to the vacuole. J Cell Biol 1997; 138:517-29; PMID:9245783; http://dx.doi.org/10.1083/jcb.138.3.517

[14] Ishihara N, Hamasaki M, Yokota S, Suzuki K, Kamada Y, Kihara A, Yoshimori T, Noda T, Ohsumi Y. Autophagosome requires specific early Sec proteins for its formation and NSF/SNARE for vacuolar fusion. Mol Biol Cell 2001; 12:3690-702; PMID:11694599; http://dx.doi.org/10.1091/mbc.12.11.3690

[15] Puri C, Renna M, Bento CF, Moreau K, Rubinsztein DC. Diverse autophagosome membrane sources coalesce in recycling endosomes. Cell 2013; 154:1285-99; PMID:24034251; http://dx.doi.org/10.1016/j.cell.2013.08.044

[16] Nair U, Jotwani A, Geng J, Gammoh N, Richerson D, Yen WL, Griffith J, Nag S, Wang K, Moss T, et al. SNARE proteins are required for macroautophagy. Cell 2011; 146:290-302; PMID:21784249; http://dx.doi.org/10.1016/j.cell.2011.06.022

[17] Mali P, Yang L, Esvelt KM, Aach J, Guell M, DiCarlo JE, Norville JE, Church GM. RNA-guided human genome engineering via Cas9. Science 2013; 339:823-6; PMID:23287722; http://dx.doi.org/10.1126/science.1232033

[18] Wendler F, Tooze S. Syntaxin 6: the promiscuous behaviour of a SNARE protein. Traffic (Copenhagen, Denmark) 2001; 2:606-11; PMID:11555414; http://dx.doi.org/10.1034/j.1600-0854.2001.20903.x

[19] Perera HK, Clarke M, Morris NJ, Hong W, Chamberlain LH, Gould GW. Syntaxin 6 regulates Glut4 trafficking in 3T3-L1 adipocytes. Mol Biol Cell 2003; 14:2946-58; PMID:12857877; http://dx.doi.org/10.1091/mbc.E02-11-0722

[20] Kuliawat R, Kalinina E, Bock J, Fricker L, McGraw TE, Kim SR, Zhong J, Scheller R, Arvan P. Syntaxin-6 SNARE involvement in secretory and endocytic pathways of cultured pancreatic β-cells. Mol Biol Cell 2004; 15:1690-701; PMID:14742717; http://dx.doi.org/10.1091/mbc.E03-08-0554

[21] Choudhury A, Marks DL, Proctor KM, Gould GW, Pagano RE. Regulation of caveolar endocytosis by syntaxin 6-dependent delivery of membrane components to the cell surface. Nat Cell Biol 2006; 8:317-28; PMID:16565709; http://dx.doi.org/10.1038/ncb1380

[22] Laufman O, Hong W, Lev S. The COG complex interacts directly with Syntaxin 6 and positively regulates endosome-to-TGN retrograde transport. J Cell Biol 2011; 194:459-72; PMID:21807881; http://dx.doi.org/10.1083/jcb.201102045

[23] Longatti A, Lamb CA, Razi M, Yoshimura S, Barr FA, Tooze SA. TBC1D14 regulates autophagosome formation via Rab11- and ULK1-positive recycling endosomes. J Cell Biol 2012; 197:659-75; PMID:22613832; http://dx.doi.org/10.1083/jcb.201111079

[24] Watson RT, Pessin JE. Functional cooperation of two independent targeting domains in syntaxin 6 is required for its efficient localization in the trans-golgi network of 3T3L1 adipocytes. J Biol Chem 2000; 275:1261-8; PMID:10625671; http://dx.doi.org/10.1074/jbc.275.2.1261

[25] Moore ER, Mead DJ, Dooley CA, Sager J, Hackstadt T. The trans-Golgi SNARE syntaxin 6 is recruited to the chlamydial inclusion membrane. Microbiology 2011; 157:830-8; PMID:21109560; http://dx.doi.org/10.1099/mic.0.045856-0

[26] Kabeiseman EJ, Cichos KH, Moore ER. The eukaryotic signal sequence, YGRL, targets the chlamydial inclusion. Frontiers Cell Infect Microbiol 2014; 4:129; PMID:25309881; http://dx.doi.org/10.3389/fcimb.2014.00129

[27] Murray RZ, Wylie FG, Khromykh T, Hume DA, Stow JL. Syntaxin 6 and Vti1b form a novel SNARE complex, which is up-regulated in activated macrophages to facilitate exocytosis of tumor necrosis Factor-α. J Biol Chem 2005; 280:10478-83; PMID:15640147; http://dx.doi.org/10.1074/jbc.M414420200

[28] Manderson AP, Kay JG, Hammond LA, Brown DL, Stow JL. Subcompartments of the macrophage recycling endosome direct the differential secretion of IL-6 and TNFalpha. J Cell Biol 2007; 178:57-69; PMID:17606866; http://dx.doi.org/10.1083/jcb.200612131

[29] Hulce JJ, Cognetta AB, Niphakis MJ, Tully SE, Cravatt BF. Proteome-wide mapping of cholesterol-interacting proteins in mammalian cells. Nat Methods 2013; 10:259-64; PMID:23396283; http://dx.doi.org/10.1038/nmeth.2368

[30] Reverter M, Rentero C, Garcia-Melero A, Hoque M, Vila de Muga S, Alvarez-Guaita A, Conway J R.W, Wood P, Cairns R, Lykopoulou L, et al. Cholesterol regulates Syntaxin 6 trafficking at trans-Golgi network endosomal boundaries. Cell Reports 2014; 7:883-97; PMID:24746815; http://dx.doi.org/10.1016/j.celrep.2014.03.043

[31] Mounier J, Boncompain G, Senerovic L, Lagache T, Chretien F, Perez F, Kolbe M, Olivo-Marin JC, Sansonetti PJ, Sauvonnet N. Shigella effector IpaB-induced cholesterol relocation disrupts the Golgi complex and recycling network to inhibit host cell secretion. Cell Host Microbe 2012; 12:381-9; PMID:22980334; http://dx.doi.org/10.1016/j.chom.2012.07.010

[32] Taylor SD, Sanders ME, Tullos NA, Stray SJ, Norcross EW, McDaniel LS, Marquart ME. The cholesterol-dependent cytolysin pneumolysin from Streptococcus pneumoniae binds to lipid raft microdomains in human corneal epithelial cells. PLoS One 2013; 8:e61300; PMID:23577214; http://dx.doi.org/10.1371/journal.pone.0061300

[33] Bhakdi S, Bayley H, Valeva A, Walev I, Walker B, Kehoe M, Palmer M. Staphylococcal α-toxin, streptolysin-O, and Escherichia coli hemolysin: prototypes of pore-forming bacterial cytolysins. Arch Microbiol 1996; 165:73-9; PMID:8593102; http://dx.doi.org/10.1007/s002030050300

[34] Kreykenbohm V, Wenzel D, Antonin W, Atlachkine V, von Mollard GF. The SNAREs vti1a and vti1b have distinct localization and SNARE complex partners. Eur J Cell Biol 2002; 81:273-80; PMID:12067063; http://dx.doi.org/10.1078/0171-9335-00247

[35] Guo B, Liang Q, Li L, Hu Z, Wu F, Zhang P, Ma Y, Zhao B, Kovács AL, Zhang Z, et al. O-GlcNAc-modification of SNAP-29 regulates autophagosome maturation. Nat Cell Biol 2014; 16:1215-26; PMID:25419848; http://dx.doi.org/10.1038/ncb3066

[36] Mizushima N. Sugar modification inhibits autophagosome-lysosome fusion. Nat Cell Biol 2014; 16:1132-3; PMID:25434465; http://dx.doi.org/10.1038/ncb3078

[37] Oda S, Nozawa T, Nozawa-Minowa A, Tanaka M, Aikawa C, Harada H, Nakagawa I. Golgi-resident GTPase Rab30 promotes the biogenesis of pathogen-containing autophagosomes. PLoS One 2016; 11:e0147061; PMID:26771875; http://dx.doi.org/10.1371/journal.pone.0147061